

Staged modulation using synergistic alkaline biochar-ferrate enhances medium-chain fatty acid production from waste activated sludge

Received: 18 May 2025

Accepted: 11 November 2025

Cite this article as: Wang, Y., Ji, Y., Luo, X. *et al.* Staged modulation using synergistic alkaline biochar-ferrate enhances medium-chain fatty acid production from waste activated sludge. *Commun Eng* (2025). <https://doi.org/10.1038/s44172-025-00558-4>

Yufen Wang, Ya Ji, Xiaofeng Luo, Tingting Zhu, Bing-Jie Ni & Yiwen Liu

We are providing an unedited version of this manuscript to give early access to its findings. Before final publication, the manuscript will undergo further editing. Please note there may be errors present which affect the content, and all legal disclaimers apply.

If this paper is publishing under a Transparent Peer Review model then Peer Review reports will publish with the final article.

1 **Staged modulation using synergistic alkaline biochar-ferrate**
2 **enhances medium-chain fatty acid production from waste**
3 **activated sludge**

4 Yufen Wang^a, Ya Ji^a, Xiaofeng Luo^a, Tingting Zhu^a, Bing-Jie Ni^b, Yiwen Liu^{a,*}

5

6 ^a School of Environmental Science and Engineering, Tianjin University, Tianjin 300072,

7 China

8 ^b School of Civil and Environmental Engineering, University of New South Wales,

9 Sydney, New South Wales, 2052, Australia

10

11

12

13 *Corresponding author

14 E-mail: yiwen.liu@tju.edu.cn (Y. Liu)

15 Abstract

16 Medium-chain fatty acids (MCFAs) are carbon-neutral alternative to petroleum-
17 derived chemicals, offering sustainable valorization for waste activated sludge. Current
18 bioproduction systems, however, face a critical dual bottleneck stemming from
19 complex sludge matrices and inefficient carbon flux regulation. Here, we develop a
20 stage-optimized modulation strategy employing alkaline biochar (AlkBC)-ferrate to
21 sequentially enhance sludge solubilization and targeted MCFA-producing fermentation.
22 Maximum MCFA production reaches 10495.0 mg chemical oxygen demand L⁻¹, 20.6-,
23 15.2- and 2.3-fold higher than the control, AlkBC-alone and ferrate-alone groups,
24 respectively. Mechanistically, AlkBC initiates ferrate activation to produce metastable
25 Fe(IV)/Fe(V) intermediates via physical adsorption, electron donation, and oxygen-
26 functionalized coordination. High-valent Fe species oxidation coupled with AlkBC-
27 elevated alkalinity efficiently disrupts sludge polymerized structure and drives
28 bioconversion of released organics. Simultaneously, AlkBC is structurally reconfigured
29 due to ferrate oxidation with surface-loaded Fe₂O₃ as active component, substantially
30 enhancing chain elongation. Furthermore, AlkBC-ferrate enriches key functional
31 bacteria while suppressing methanogens, steering carbon flux towards MCFA
32 production.

33 Keywords

34 Medium-chain fatty acids (MCFAs); Ferrate; Alkaline biochar (AlkBC); Chain
35 elongation; Fe(IV)/Fe(V)

36 Introduction

37 The inevitable generation of waste activated sludge (WAS) from wastewater
38 treatment imposes escalating environmental burdens^{1,2}. To address this challenge, an
39 emerging strategy integrating anaerobic fermentation with chain elongation has been
40 proposed, efficiently converting sludge organics into versatile, high-value medium-
41 chain fatty acids (MCFAs, C6–C12 monocarboxylic acids) for sustainable waste
42 valorization^{3,4}. Crucially, MCFA biosynthesis contributes to CO₂ mitigation, as
43 approximately 30% of the carbon in chain-elongating biomass derives from CO₂
44 fixation^{5,6}. Nevertheless, WAS-derived MCFA production remains constrained by
45 inefficient sludge degradation, suboptimal electron transfer, and competing metabolic
46 pathways⁷.

47 Ferrate (Fe^{VI}O₄²⁻), a multifunctional strong oxidant, combines chemical oxidation,
48 coagulation, and disinfection capabilities⁸. It plays an important role in organic
49 pollutant removal, pathogen inactivation, and sludge treatment^{9,10}. The reactive Fe
50 species in ferrate-based systems include Fe(VI), Fe(IV), and Fe(V)¹¹. Among these,
51 Fe(IV) ($E^0=1.0-1.4$ V) and Fe(V) ($E^0=1.7$ V) exhibit substantially higher reactivity than
52 Fe(VI) ($E^0=0.7$ V) under alkaline conditions¹². Our prior work revealed that ferrate
53 pretreatment substantially improved sludge solubilization and organic matter release,
54 achieving maximum MCFA yield of 8106.3 mg chemical oxygen demand (COD) L⁻¹¹³.
55 Notably, iron oxides (e.g., Fe₂O₃) from ferrate reduction could serve as effective
56 electron conduits during anaerobic sludge fermentation¹⁴⁻¹⁶. However, rapid self-decay
57 of ferrate in aqueous systems reduces high-valent Fe species availability, diminishing

58 its oxidative efficiency towards WAS organic components and increasing operational
59 costs^{17,18}.

60 Biochar (BC) is a conductive carbon material produced through high-temperature
61 carbonization of organic waste¹⁹. Its aromatic functional groups (e.g., quinone, phenolic
62 and hydroquinone moieties) exhibit redox activity, enabling participation in advanced
63 oxidation processes and mediation of extracellular electron transfer^{20,21}. BC addition
64 substantially enhances MCFA production from WAS alkaline fermentation liquor or
65 raw sludge by improving electron transfer efficiency^{22,23}. Notably, the pH of BC
66 depends on feedstock origin, with some types like banana peel-derived BC exhibiting
67 alkaline properties²⁴. Although the inherent alkalinity of alkaline BC (AlkBC) benefits
68 WAS solubilization and hydrolysis, it requires high doses (15–25 g L⁻¹) to attain
69 considerable organic release during pretreatment²⁵. To reduce dosage requirements of
70 sole pretreatment and mitigate high-valent Fe species self-decomposition, we propose
71 integrating AlkBC with ferrate for WAS pretreatment. This integrated strategy shows
72 potential for enabling stage-optimized modulation of sludge-to-MCFA conversion.
73 Specifically, AlkBC would enhance ferrate pretreatment for sludge disintegration, with
74 the resulting AlkBC-Fe(III) composites serving as highly efficient electron conduits
75 during fermentation.

76 This study systematically evaluated the efficacy of AlkBC-ferrate in enhancing
77 MCFA production and suppressing competitive pathways through comprehensive
78 analysis of gas and liquid phase products. Mechanistic investigations were conducted
79 on the two-stage process, namely sludge pretreatment and targeted MCFA-producing

80 fermentation. First, the effects of AlkBC-ferrate on sludge polymerization structures
81 and organics release were elucidated, identifying the key drivers behind its role in
82 promoting chemical decomposition and bioconversion of macromolecular organics.
83 Second, ferrate modification of AlkBC was confirmed by characterizing functional
84 group alterations, surface iron oxide composition, and Fe(III)-AlkBC composite
85 microstructure, with subsequent assessment of the modified material's impact on chain
86 elongation. Furthermore, microbial communities were analyzed using 16S rRNA high-
87 throughput sequencing to elucidate modulation of microbial composition and
88 abundances by AlkBC-ferrate.

89 **Methods**

90 **Sources of WAS, inoculum and AlkBC**

91 The WAS was sourced from a secondary sedimentation tank in Tianjin, with its
92 main properties listed in Supplementary Table 1. The inoculum was cultured using WAS
93 as substrate and ethanol as electron donor (Supplementary Table 1). AlkBC was
94 prepared by carbonizing banana peel at high temperature, with the steps detailed in
95 Supplementary Text 1. The recovery efficiency of AlkBC was 33.7%. The pH of its
96 aqueous suspension (5 g L^{-1}) was 10.22 ± 0.13 , determined using a calibrated pH meter.

97 **AlkBC-ferrate pretreatment and MCFA production**

98 Batch experiments were conducted in 300 mL bioreactors ($V=300 \text{ mL}$), designated
99 as control, AlkBC, ferrate or AlkBC-ferrate, and each was loaded with 150 mL WAS.
100 The experimental groups were supplemented with 5 g L^{-1} AlkBC, 0.15 g potassium
101 ferrate per g total suspended solids (TSS), or a combination of both (5 g L^{-1} AlkBC +

102 0.15 g potassium ferrate per g TSS). These dosages were notably lower than those
103 reported in previous studies^{13,18,22}. All reactors were incubated at medium temperature
104 with reciprocal shaking (120 rpm) for 2 days to facilitate sludge solubilization and
105 biochemical conversion of organic matter. Following pretreatment, the sludge pH was
106 adjusted to 6.5 ± 0.1 before sequential addition of 15 mL inoculum and 160 mM ethanol.
107 Prior to ethanol supplementation, the reactors were purged with N₂ to maintain
108 anaerobic conditions. Finally, the sealed reactors were transferred to a temperature-
109 controlled incubator (35 °C, 120 rpm) for MCFA production via anaerobic fermentation.
110 All experiments were conducted in triplicate.

111 **Impact identification of AlkBC-ferrate on WAS dissolution and organics** 112 **conversion**

113 To elucidate the enhancement effect of AlkBC in ferrate pretreatment, the
114 dissolution and conversion of solid organic matter in sludge was firstly investigated. At
115 2, 6, 12, 24 and 48 hours during the pretreatment, liquid samples were collected from
116 the control, AlkBC, ferrate and AlkBC-ferrate reactors, and concentrations of dissolved
117 substrates and hydrolysis-acidification products were detected. To recognize the
118 influence of AlkBC-ferrate on sludge polymerization structures, the bound extracellular
119 polymeric substances (EPS), i.e., tightly-bound EPS and loosely-bound EPS, were
120 obtained by a heat-extracted method²⁶. The release and decomposition of extracellular
121 macromolecular organic matter were evaluated by analyzing changes in functional
122 group structures and proteinic secondary structures in the WAS supernatant²⁷. The
123 ability of hydrolytic bacteria to degrade released organics was examined by hydrolase

124 activities²⁸. Further, the potential action of AlkBC on biotransformation of dissolved
125 macromolecular organics in the AlkBC-ferrate system was assessed by synthetic
126 wastewater experiments^{4,29}, as detailed in Supplementary Text 2.

127 **Elucidating the mechanism of AlkBC enhancing ferrate pretreatment**

128 After ferrate and AlkBC addition, the pH value of WAS increased immediately,
129 and then gradually decreased (Supplementary Fig. 4a). The maximum pH values
130 reached 9.35 in the ferrate reactor and 9.75 in the AlkBC-ferrate reactor. To elucidate
131 the mechanism of AlkBC-enhanced ferrate pretreatment, the individual contributions
132 of alkaline condition and oxidation to sludge dissolution were quantified. Specifically,
133 eight groups were set up in this experiment, i.e., control, pH=9.35, pH=9.75, AlkBC,
134 ferrate, AlkBC-ferrate, ferrate (60 min) and AlkBC-ferrate (60 min). Among them,
135 pH=9.35 or pH=9.75 were respectively aimed to describe the alkaline effect of ferrate
136 or AlkBC-ferrate. While ferrate (60 min) or AlkBC-ferrate (60 min) indicated that
137 ferrate or AlkBC-ferrate oxidized WAS for 60 min, and then the pH value was adjusted
138 to neutral. Accordingly, the activation of AlkBC on ferrate reaction could be assessed
139 by organics release from WAS after pretreatment. Additionally, Fe(VI), Fe(V) and
140 Fe(IV) were measured to further clarify the role of AlkBC in ferrate oxidation.

141 **Revealing the variations in physicochemical properties of AlkBC and potential** 142 **effect of ferrate-modified AlkBC on chain elongation biostep**

143 Ferrate oxidation may alter the surface functional groups and characteristics of
144 AlkBC, such as redox capacity and adsorption property. Besides, ferrate-reduced
145 particles (i.e., iron (hydr)oxide) would be loaded onto the AlkBC surface to reduce the

146 specific surface area and increase electron transfer activity. After AlkBC-ferrate
147 pretreatment, ferrate-modified AlkBC will enter the sludge fermentation system, posing
148 a potential impact on chain elongation (i.e., the essential bioprocess for MCFA
149 generation). Consequently, the physicochemical properties of raw AlkBC and Fe(VI)-
150 modified AlkBC were investigated by scanning electron microscopy, X-ray
151 photoelectron spectroscopy and Fourier-transform infrared spectroscopy. The chain
152 elongation experiment was conducted in six bioreactors, including control, raw AlkBC,
153 ferrate-reduced particles, ferrate-modified AlkBC, Fe(OH)₃, raw AlkBC-Fe(OH)₃. The
154 preparation of ferrate-reduced particles and ferrate-modified AlkBC, and details of
155 chain elongation experiment were described in Supplementary Text 3.

156 **16S rRNA high-throughput sequencing**

157 The alterations in bacterial and archaeal communities induced by AlkBC-ferrate
158 were elucidated through 16S rRNA high-throughput sequencing. At the end of
159 anaerobic fermentation (Section of *AlkBC-ferrate pretreatment and MCFA production*),
160 10 mL sludge mixture was separately extracted from the control, AlkBC, ferrate and
161 AlkBC-ferrate reactors. DNA was extracted from the sludge samples using the FastPure
162 Soil DNA Isolation Kit (MJYH, shanghai, China), and qualified by 1.0% agarose gel
163 electrophoresis. The hypervariable region V4 of microbial 16S rRNA gene were
164 amplified with forward primer 515FmodF (GTGYCAGCMGCCGCGGTAA) and
165 reverse primer 806RmodR (GGACTACNVGGGTWTCTAAT) by Applied Biosystems
166 GeneAmp® 9700 PCR system. After purification, the amplification products were used
167 for library construction and sequenced on the Illumina Nextseq 2000 platform at Major

168 Bio. (Shanghai, China). Operational taxonomic units were clustered from the optimized
169 sequences using UPARSE (version 7.1) at a 97% similarity threshold. The
170 representative sequences of operational taxonomic units were taxonomically classified
171 using the RDP classifier (version 2.11) against the 16S rRNA gene database (SILVA,
172 version 138) with a confidence threshold of 70%. The raw sequencing data have been
173 deposited in the Sequence Read Archive database at NCBI under accession number
174 PRJNA1346931.

175 **Analytical methods**

176 Volatile/total (suspended) solids and ammonia nitrogen were measured by the
177 standard methods³⁰. Proteins, carbohydrates and COD were respectively quantified
178 using the Lowry-Folin method, Anthrone-H₂SO₄ method and HACH test kits^{31,32}. The
179 functional groups of AlkBC and released organics were characterized by Fourier-
180 transform infrared spectrometer (Nicolet iS5)²². The chemical nature of C and Fe on
181 AlkBC was examined by X-ray photoelectron spectroscopy (Thermo Scientific Escalab
182 250Xi)³³. The microscopic morphology of raw AlkBC and ferrate-modified AlkBC, and
183 interactions of microorganisms-iron oxides-biochar were analyzed by scanning electron
184 microscopy³⁴. Electron transport system activity was assessed following previous
185 methodology³⁵. Fe(VI), Fe(V) and Fe(IV) in the AlkBC-ferrate oxidation process were
186 measured by ultraviolet-visible spectroscopy^{36,37}. MCFAs, short-chain fatty acids
187 (SCFAs) and alcohols were detected by a gas chromatograph (GC-2014, SHIMADZU).
188 The volumes and contents of gas phase products (i.e., hydrogen and methane) were
189 measured using the drainage method and a gas chromatography (SP-7890 Plus, Lunan),

190 respectively.

191 **Results**

192 **Performance of MCFA biosynthesis from WAS fermentation driven by AlkBC-** 193 **ferrate**

194 The MCFA concentration gradually increases with fermentation time and almost
195 reaches a stable state after 12 days (Fig. 1a). The maximum MCFA production in the
196 control and AlkBC reactors is only 486.3 and 647.7 mg COD L⁻¹, respectively. This
197 contrasts with a previous study reporting 4800–5700 mg COD L⁻¹ of MCFA production
198 from WAS alkaline fermentation liquor with BC addition²². The low MCFA output in
199 the control and AlkBC groups may be attributed to insufficient electron acceptors
200 directly available for chain elongation reactions, as evidenced by limited increase in
201 soluble chemical oxygen demand (SCOD) after fermentation (Supplementary Fig. 1a).
202 Also, potentially competing microorganisms may occupy higher ecological niches in
203 these two reactors, rendering chain elongation bacteria at a competitive disadvantage.
204 Methanogens are the main competitor for MCFA production via open-culture
205 fermentation, and would cause electron acceptor (i.e., SCFA) depletion or hydrogen
206 partial pressure reduction, posing adverse impacts on chain elongation step⁷.
207 Accordingly, the roles of AlkBC-ferrate in controlling methanogenesis and improving
208 elongating bacterial activity could be respectively reflected by methane and hydrogen
209 production in Fig. 1b and Supplementary Fig. 1b. After ferrate pretreatment, MCFA
210 production increases to 3212.2 mg COD L⁻¹, similar to our previous study¹³. However,
211 AlkBC-ferrate pretreatment results in a dramatic increase in MCFA production, which

212 eventually reaches 10495.0 mg COD/L, a 20.6-, 15.2- and 2.3-fold enhancement over
213 the control, AlkBC alone and ferrate alone, respectively.

214 As shown in Fig. 1c, butyric acid is the primary product in the control or single-
215 treatment groups, while caproic acid dominates the liquid-phase products in the AlkBC-
216 ferrate group. Specifically, MCFAs proportion for the control, AlkBC and ferrate is
217 respectively 3.7%, 4.7% and 19.7%, whereas it increases markedly to 62.8% by AlkBC-
218 ferrate. It indicates that AlkBC-ferrate can lead to a higher conversion preference
219 towards MCFAs, consistent with the increased conversion efficiency in Supplementary
220 Fig. 1a. Long-chain alcohols (i.e., butanol and hexanol) are major byproducts of chain
221 elongation reactions. They may originate from the reduction of chain elongation
222 products or intermediates, such as butyryl/caproyl coenzyme A and butyric/caproic acid,
223 leading to waste of electron donors³⁸. In Fig. 1d, maximum concentration of long-chain
224 alcohols for the control reaches 5229.6 mg COD L⁻¹, while it reduces to 4785.5, 3485.7
225 and 1160.6 mg COD L⁻¹ at AlkBC, ferrate and AlkBC-ferrate, respectively, implying
226 increased inhibitions of the microorganisms producing these alcohols with pretreatment
227 intensity. These findings collectively enclose that AlkBC-ferrate efficiently suppresses
228 the competitive metabolisms against chain elongation process, facilitates conversion of
229 more substrates to MCFAs, and saves the cost for methanogen inhibitor dose.

230 Fig. 1

231 **Phase transfer and bioavailability evolution of particulate organic matter**
232 **triggered by AlkBC-ferrate pretreatment**

233 EPS, formed by microbial growth, maintains the mechanical stability of sludge

234 flocs and impede the leaching of intracellular organic matter³⁹. Thereby, disruption of
235 sludge polymeric structure is an indispensable step to promote solid-phase organics
236 release, sludge degradation and electron acceptor generation⁴⁰. As shown in Fig. 2a,
237 both ferrate and AlkBC-ferrate increase the proteins and polysaccharides contents in
238 loosely-bound EPS, whereas reduce these organics in tightly-bound EPS compared to
239 control ($p < 0.05$). For example, the protein concentration of tightly-bound EPS fraction
240 is 326.6, 353.3, 254.1 and 267.1 mg COD L⁻¹ in the control, AlkBC, ferrate and AlkBC-
241 ferrate groups, respectively. The concentrations of proteins and polysaccharides in the
242 tightly-bound EPS fraction could not be further reduced by AlkBC-ferrate, compared
243 to the ferrate-only group. This may be explained by AlkBC promoting EPS secretion
244 though functioning as an electron conduit in anaerobic environments.

245 Accordingly, the concentrations of proteins, carbohydrates and SCOD in the
246 sludge supernatant increase notably with pretreatment intensity (namely, AlkBC-
247 ferrate > ferrate > AlkBC > control) within the initial 12 hours, and then tend to stabilize
248 or decrease (Fig. 2b-2d). This indicates that the extension of pretreatment time to 48
249 hours benefits hydrolysis and acidification of released organics. Specially, SCOD
250 content attains 5450 mg COD L⁻¹ after AlkBC-ferrate pretreatment, elevating by
251 564.6%, 249.4%, 36.3% than the control, AlkBC and ferrate, respectively. Additionally,
252 the total SCOD of extracellular organics in the AlkBC-ferrate group is considerably
253 higher than that of the control, AlkBC or ferrate (Fig. 2d), implying more severe cell
254 leakage induced by the combination technique. These results prove that AlkBC-ferrate
255 further accelerates sludge floc disruption and particulate organic matter release,

256 providing abundant soluble organic components for subsequent hydrolysis,
257 acidification and chain elongation processes.

258 **Fig. 2.**

259 Proteins are the main organic components in sludge and their biodegradability is
260 affected by the spatial structure⁴¹. To elucidate the structural characteristics of released
261 proteins under different pretreatment conditions, the amide I region (1600-1700 cm⁻¹)
262 in Fourier-transform infrared spectra (Supplementary Fig. 2a) was subjected to
263 deconvolution and second-order derivative fitting⁴². It could be divided into 6 peaks,
264 including aggregated strands (peak 1), β -sheet (peak 2), random coils (peak 3), α -helix
265 (peak 4), 3-turn helix (peak 5) and antiparallel β -sheet/aggregated strands (peak 6) (Fig.
266 2e). It has been indicated that α -helix and β -sheet favor sludge flocculation⁴³, and a low
267 ratio of α -helix/(β -sheet + random coil) could be responsible for looser proteinic
268 structure⁴⁴. As shown in Supplementary Fig. 2b, the proportion of proteinic secondary
269 structure obviously changes with pretreatment conditions. The ratios of α -helix and β -
270 sheet are 34.2%, 33.2%, 31.4% and 27.6% for the control, AlkBC, ferrate and AlkBC-
271 ferrate, respectively, presenting a decreasing trend. Likewise, the proportion of α -
272 helix/(β -sheet + random coil) is reduced from 69.7% (control) to 57.8% (AlkBC), 51.4%
273 (ferrate) or 49.2% (AlkBC-ferrate). The structure of random coil may be also destructed
274 by AlkBC-ferrate, resulting in no further obvious reduction of this ratio. Collectively,
275 AlkBC-ferrate pretreatment predominantly disrupts hydrogen bonding networks
276 critical for α -helix and β -sheet integrity, thereby exposing proteolytic cleavage sites and
277 enhancing substrate bioavailability for fermentative microbial consortia. The

278 fluorescence response values of released organics in the AlkBC-ferrate system
279 demonstrate parity with or marginal reduction compared to the ferrate-only system
280 during pretreatment (Supplementary Fig. 3). This phenomenon is likely due to the
281 intensified oxidative dismantling of fluorescent moieties through synergistic AlkBC-
282 ferrate interactions. This mechanistic behavior substantiates its superior capability in
283 chemically decomposing macromolecular organics, as evidenced by the structural
284 disintegration of α -helix and β -sheet conformations integral to sludge stability.

285 Degradable components in the supernatant of pretreated sludge include organic
286 macromolecules, hydrolysis products, other intermediates and SCFAs. Thus, the
287 biotransformation of macromolecular substrates in WAS can be readily reflected by
288 hydrolase activity and degradation product content. After pretreatment, protease, α -
289 glucosidase, ammonia nitrogen and SCFAs are obviously elevated by AlkBC-ferrate
290 regarding their activity or concentration (Fig. 2f). For example, AlkBC-ferrate improves
291 protease activity and SCFA production by 23.1% and 32.7%, respectively, in
292 comparison with ferrate alone. These results demonstrate that AlkBC-ferrate
293 accelerates SCFA generation by driving the chemical decomposition and
294 biotransformation of soluble macromolecular organics, thereby increasing electron
295 acceptor availability for chain elongation.

296 **Elucidating synergistic mechanisms of AlkBC and ferrate in particulate organics** 297 **destabilization and bioavailability enhancement during WAS pretreatment**

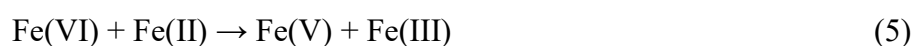
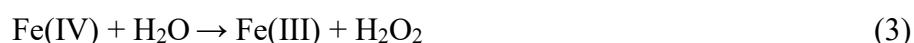
298 The pH value of WAS largely varies with pretreatment conditions and reaction
299 time (Supplementary Fig. 4a). After 30 minutes, the AlkBC, ferrate and AlkBC-ferrate

300 reactors reach their respective maximum pH, i.e., 8.09, 9.35 and 9.75. Notably, AlkBC
301 addition results in an increase of pH, which may further facilitate WAS dissolution, and
302 assure effective sludge oxidation via weakening ferrate self-decomposition.

303 To elucidate the mechanism of AlkBC enhancing ferrate pretreatment, the
304 respective contributions of alkalinity and oxidation to sludge dissolution were
305 distinguished (Fig. 3a-3b). The pH9.35 and pH9.75 series represent the alkalinity
306 induced by ferrate and AlkBC-ferrate, while [ferrate(1h)] and [AlkBC-ferrate(1h)] refer
307 to their oxidizing effects, respectively. The variations in soluble protein concentrations
308 with pretreatment conditions demonstrate that both alkalinity and oxidation critically
309 drive sludge disintegration in the ferrate and AlkBC-ferrate systems (Fig. 3a). After 12
310 hours of pretreatment, the oxidation effects of ferrate and AlkBC-ferrate increase SCOD
311 concentration by 1080 mg L⁻¹ and 2360 mg L⁻¹, respectively, as calculated by
312 subtracting the alkaline contributions (Fig. 3b). Such increment (i.e., 2360-1080=1280
313 mg L⁻¹) is close to the difference (i.e., 1190 mg L⁻¹ of SCOD) between [ferrate(1h)] and
314 [AlkBC-ferrate(1h)], demonstrating that AlkBC enhances ferrate oxidation.

315 Ferrate (Fe(VI)) is unstable in water and will self-decay into Fe(IV), Fe(V) and
316 H₂O₂, with Fe(III) and O₂ as the final forms⁴⁵. During the ferrate self-decomposition
317 process, Fe(V) and Fe(IV) may self-decay to Fe(III), while H₂O₂ also converts Fe(IV)
318 and Fe(V) to Fe(II) and Fe(III), respectively, as shown in Eqs. (1)-(11)^{11,46}. Apparently,
319 the excessive self-decomposition of high-valent Fe intermediates would decrease the
320 oxidation capacity of ferrate¹⁷. Thereby, ferrate activation and extension of Fe(V)/Fe(IV)
321 lifetime can boost the efficiency of sludge treatment by ferrate. The ultraviolet-visible

322 absorbance of dissolved ferrate is rapidly reduced by AlkBC (Supplementary Fig. 4b).
 323 After 1 hour, Fe(VI) ($\lambda_{\text{max}}=510$ nm) decreases by 20.3% in the ferrate group, but it
 324 decreases by 90.7% in the AlkBC-ferrate group (Fig. 3c). Fe(V) and Fe(IV) have been
 325 reported to have the maximum absorbance at 380 nm and 420 nm, respectively^{36,37}.
 326 Soluble Fe(III) is present as $\text{Fe}(\text{OH})_2^+$ and its maximum absorbance in the ultraviolet-
 327 visible spectrum occurs at ca. 305 nm when pH is greater than 5⁴⁷. Thereby, the strong
 328 absorption peaks at near 300 nm, 370 nm and 435 nm in the AlkBC-ferrate system are
 329 related to produced Fe(III), Fe(V) and Fe(IV), respectively (Fig. 3c and Supplementary
 330 Fig. 4b). The intensity of absorption peaks reflects that AlkBC-ferrate produces more
 331 Fe(V)/Fe(IV) species than ferrate alone. The mechanism of AlkBC activating ferrate
 332 oxidation may involve two steps. First, Fe(VI) is physically adsorbed onto the surface
 333 of biochar, as supported by its rapid decrease (by 60%) after 10 min of reaction. Then,
 334 Fe(VI) reacts with electron-rich aromatic moieties on AlkBC to transfer into metastable
 335 biochar-complexes or free Fe(V)/Fe(IV)⁴⁸. Accordingly, these high-valent Fe
 336 intermediates in the AlkBC-ferrate system are more efficient for WAS disintegration
 337 due to the higher pH value (i.e., alleviation of self-decay) and the presence of ligand
 338 (i.e., AlkBC surfaces)⁴⁶.





339

Fig. 3

340 Beyond chemical mechanisms, AlkBC-ferrate reaction products likely act as
 341 driving forces to stimulate the metabolic activity of functional bacteria and promote
 342 biodegradation of released organic matter. Fig. 3d shows the changes in the degradation
 343 extent of bovine serum albumin and acidification efficiency of small organic molecules
 344 (i.e., amino acids and glucose) with/without AlkBC addition. Due to the presence of
 345 AlkBC, the degradation efficiency of bovine serum albumin increases from 57.8% to
 346 70.0% after 72 hours, while SCFA production rises from 1795.5 to 3319.8 mg COD L⁻¹
 347 after 48 hours. Additionally, Fe(III) produced by ferrate reduction could also promote
 348 the hydrolyzing and acidifying of organic matter through dissimilatory Fe reduction
 349 process¹⁶. Therefore, the increased alkalinity and AlkBC-activated ferrate oxidation are
 350 responsible for sludge dissolution and structural decomposition of released organics,
 351 while the AlkBC-ferrate reaction products trigger biological effects to enhance
 352 biodegradation of soluble organic matter.

353 Ferrate-induced AlkBC modification and its catalytic role in chain elongation

354 The ability of biochar facilitating electron transfer is closely related to its surface
 355 functional group structure and supported metal oxides. Previous research showed that

356 chemical oxidation treatment (e.g., with H_2O_2) could modify biochar, increasing
357 oxygen-containing functional groups on its surface and enhancing redox properties and
358 electron transport capacity⁴⁹. It was suggested that ferrate decomposition in water
359 resulted in the formation of nanoparticles that had core-shell nanoarchitecture with γ -
360 Fe_2O_3 as core and γ - FeOOH as shell¹⁴. Thereby, the physicochemical property of
361 AlkBC may be modified due to ferrate oxidation and formation of Fe(III) particles,
362 posing potential impacts on the subsequent fermentation process, especially chain
363 elongation.

364 The Fourier-transform infrared spectra in Fig. 4a reveal changes in major
365 functional groups of AlkBC before and after ferrate oxidation. The characteristic peaks
366 at 1110 cm^{-1} , 1570 cm^{-1} and 3430 cm^{-1} are separately related with C-O, C=O and C-OH
367 functional groups²², and their intensities are greatly enhanced under ferrate oxidation,
368 implying an increase of C-O and C=O on the AlkBC surface. The bonding state of
369 carbon elements is also verified by C1s spectra obtained from X-ray photoelectron
370 spectroscopy (Fig. 4b-4c). It could be divided to three peaks with binding energies of
371 284.8, 286 and 288.5 eV, individually representing C-C, C-O and C=O groups²². After
372 ferrate oxidation, C-C decreases from 77.4% to 70.2%, while C-O increases from 9.3%
373 to 17.7%. As exhibited by scanning electron microscopy micrographs in Supplementary
374 Fig. 5, the morphology of AlkBC becomes blurred and iron oxides are loaded onto its
375 surface after ferrate oxidation. Obviously, ferrate oxidation alters the microstructure of
376 AlkBC and increases oxygen-containing functional groups, which enhances
377 adsorption-binding effect with iron oxides to further improve the reactivity and electron

378 transfer capacity of AlkBC. In the Fe 2p_{3/2} and Fe 2p_{1/2} regions, the characteristic peaks
379 at 711.3 eV/724.9 eV, 719.46 eV/733.6 eV and 713.19 eV/726.79 eV correspond to
380 Fe₂O₃, Fe(III) satellite peak and Fe(OH)₃ (Fig. 4d), respectively^{15,50}, suggesting ferrate-
381 induced formation of Fe₂O₃. Based on the peaks in Fe 2p_{3/2}, it can be calculated that
382 Fe₂O₃ predominates in the Fe(III) particles on AlkBC surface, accounting for 65.9%.
383 Additionally, the absorption peaks near 561 cm⁻¹ and 462 cm⁻¹ (Fig. 4a) of ferrate-
384 modified AlkBC could also be attributed to F-O bonds in Fe₂O₃¹⁵. Our previous studies
385 demonstrated that Fe₂O₃ addition substantially increased MCFA production mainly
386 through facilitating electron transfer of chain elongation step¹⁶. It was revealed that
387 Fe₂O₃-modified digestate BC prepared via co-precipitation or impregnation exhibited
388 superior performance to Fe₂O₃ or raw BC in facilitating electron transfer and methane
389 production during anaerobic digestion of kitchen waste⁵¹.

390 After pretreatment, ferrate-modified AlkBC enters WAS fermentation reactor,
391 exerting potential impact on electron transfer capacity and chain elongation
392 performance. As shown Fig. 4e, AlkBC, ferrate and AlkBC-ferrate increase the electron
393 transfer system activity of WAS fermentation system by 26.6%, 75.5% and 237.8%,
394 respectively, compared to the control. The intensity of redox peaks in cyclic
395 voltammetry curves (Supplementary Fig. 4c) is increased by both AlkBC and ferrate,
396 but it is higher in the AlkBC-ferrate group, indicating that ferrate-modified AlkBC
397 accelerates the redox reaction and triggers faster extracellular electron transfer during
398 sludge fermentation⁵². The semi-conductive Fe₂O₃ loaded on AlkBC can further
399 promote microbial aggregation and increase their electrical connectivity by interacting

400 with electronegative EPS, establishing a microenvironment conducive to functional
401 microorganism enrichment and extracellular electron transfer (Fig. 4g). Furthermore,
402 Fig. 4f presents the MCFA production during 9 days of chain elongation with different
403 substance additions, i.e., raw AlkBC, ferrate-reduced particles, ferrate-modified AlkBC,
404 $\text{Fe}(\text{OH})_3$ and AlkBC- $\text{Fe}(\text{OH})_3$. MCFA concentration is 4857.9 mg COD L⁻¹ in the
405 control group on day 9, and it largely increases to 7852.5 and 9089.8 mg COD L⁻¹ by
406 raw AlkBC and ferrate-reduced particles, respectively. Expectedly, ferrate-modified
407 AlkBC further enhances MCFA concentration to 10200.4 mg COD L⁻¹, significantly
408 higher than the control ($p < 0.001$), raw AlkBC ($p = 0.002$) and ferrate-reduced particles
409 ($p = 0.028$). Interestingly, MCFA generation is inhibited to some degree when ferrate-
410 reduced particles are fully replaced by $\text{Fe}(\text{OH})_3$. Thus, Fe_2O_3 is the active Fe component
411 on the surface of AlkBC in accelerating electron transport and improving chain
412 elongation. These results indicate that ferrate-modified biochar more effectively
413 promotes chain elongation compared to unmodified biochar, thereby enhancing the
414 conversion of sludge-derived SCFAs to MCFAs.

415 **Fig. 4**

416 **Restructuring of microbial communities and functional taxa induced by AlkBC-**
417 **ferrate pretreatment**

418 To further reveal the mechanisms of MCFA production improvement by AlkBC-
419 ferrate, 16S rRNA high-throughput sequencing was used to investigate the alteration of
420 bacteria and archaea communities. The diversity indexes show that AlkBC-ferrate
421 reduces community richness and increases microbial diversity compared to the control

422 (Supplementary Fig. 6a). Principal coordinate analysis, based on inter-group distances,
423 reveals a distinct microbial composition in the AlkBC-ferrate group compared to the
424 other groups (Supplementary Fig. 6b). These observations suggest the presence of
425 specific microbial proliferation and non-functional microbe removal in the combined
426 group.

427 The microbial composition at the phylum level is displayed in Fig. 5a. Firmicutes
428 is a typical phylum existing in sludge fermentation system, which is closely associated
429 with sludge hydrolase secretion, SCFA production and chain elongation^{4,18}. Its
430 abundances in the control, AlkBC, ferrate and AlkBC-ferrate groups are 11.45%,
431 19.77%, 17.98% and 20.33%, respectively, indicating an apparent upward trend.
432 Euryarchaeota, a phylum of archaea containing methanogens, displays reduced
433 abundance in the ferrate and AlkBC-ferrate groups. These results demonstrate that
434 AlkBC-ferrate further promotes enrichment of functional bacteria and removal of
435 competitive archaea.

436 Fig. 5b depicts the correlation between the abundances of specific functional
437 microorganisms and pretreatment conditions at the genus level. The functional
438 microbes include hydrolyzing, acidifying and chain-elongating bacteria, such as
439 *Macellibacteroides sp.*⁵³, *Proteiniclasticum sp.*⁴, *Trichococcus sp.*⁵⁴, *Romboutsia sp.*⁵⁵,
440 *Acetoanaerobium sp.*⁴⁰. Generally, the total abundance of these microorganisms is 9.5%
441 for control, whereas it is enriched to 12.7%, 18.8% and 24.0% by AlkBC, ferrate and
442 AlkBC-ferrate, respectively. Notably, their metabolic functions (*i.e.*, hydrolysis,
443 acidification, chain elongation) may not be completely differentiated in the WAS

444 fermentation system. For example, *Macellibacteroides* is a typical hydrolyzing and
445 acid-producing genus, capable of degrading macromolecules (such as peptone and
446 cellobiose) or glucose to SCFAs and lactic acid⁵³. *Petrimonas sp.* can act as chain
447 elongation microbe⁵⁶, while its abundance is inconsistent with MCFA production,
448 implying other typical acidogens may participate in chain elongation reactions, such as
449 *Macellibacteroides sp.* and *Trichococcus sp.* Additionally, *Methanobacterium sp.*
450 belongs to hydrogenotrophic methanogens⁵⁷, which is able to decrease hydrogen partial
451 pressure and inhibit chain elongation. It accounts for 1.38% and 2.75% in the control
452 and AlkBC groups, whereas it is reduced to 0.65% and 0.04% by ferrate and AlkBC-
453 ferrate, respectively. This pronounced methanogen suppression directly correlates with
454 the >95% reduction in methane production (Fig. 1b). It is attributed to the synergistic
455 effects of elevated alkalinity and enhanced oxidizing capacity from ferrate activation,
456 both of which disrupt methanogen metabolic pathways. Thereby, AlkBC-ferrate
457 efficiently eliminates hydrogenotrophic methanogen-induced competitive inhibition on
458 chain elongation, redirecting electron flux from electron donors and acceptors towards
459 chain elongation pathways instead of methanogenesis.

460 Fig. 5

461 Discussion

462 Conversion of sludge organics into high-value MCFAs based on a staged 463 enhancement strategy

464 MCFA biosynthesis from WAS faces two critical limitations: restricted substrate
465 bioavailability and inefficient chain elongation process^{22,29}. To address these challenges,

466 this study proposes a synergistic AlkBC-ferrate pretreatment technique. Mechanism
467 investigations reveal that this strategy achieves the staged optimization of WAS-to-
468 MCFA conversion, as depicted in the schematic diagram (Fig. 6). Overall, AlkBC-
469 ferrate accelerates the release and biochemical transformation of sludge particulate
470 organics, while inhibits potential competitive microorganisms during the pretreatment
471 stage. The resulting ferrate-modified AlkBC then enters the targeted MCFA-producing
472 fermentation system to efficiently facilitate chain elongation.

473 **Fig. 6**

474 The disruption of WAS anti-hydrolysis barrier is the precondition for sludge
475 solubilization¹. After AlkBC-ferrate pretreatment, EPS structures and cell walls are
476 largely disintegrated, providing more soluble organics for functional microorganisms
477 than ferrate alone (Fig. 2a-d). With ferrate oxidation and bio-stimulation effect of
478 AlkBC, the chemical decomposition and bio-conversion of sludge particulate organics
479 are also accelerated, increasing the production of electron acceptors (i.e., SCFAs) (Fig.
480 2e-f). Further investigations reveal that the mechanisms of AlkBC enhancing ferrate
481 pretreatment include releasing alkali and activating ferrate reaction (Fig. 3b and
482 Supplementary Fig. 4a). We find that more Fe(IV) and Fe(V) are produced in AlkBC-
483 ferrate system (Supplementary Fig. 4b), suggesting the activation of ferrate reaction by
484 AlkBC⁵⁸. The activation mechanism can be interpreted as the two steps of physical
485 adsorption and electron transfer (Fig. 3c)⁴⁸, and the electron-rich groups on AlkBC
486 surface provide electron donors for ferrate reduction to high-valent Fe intermediates
487 (i.e., Fe(IV) and Fe(V))²¹. Meanwhile, the oxygen-containing functional groups on

488 AlkBC may act as ligands to increase the stability of Fe(IV)/Fe(V)⁴⁶.

489 Beyond substrate bio-availability, the potential competitive microbes can alter the
490 conversion pathways of electron donors/acceptors, causing electrons flowing to
491 byproducts such as methane, butanol and hexanol⁷. Methanogens are prevalent in
492 sludge fermentation systems, and they could cause competitive inhibition of chain
493 elongation bacteria by lowering hydrogen partial pressure and consuming
494 ethanol/acetic acid⁵⁹. Thus, substantial amounts of inhibitors are usually required to
495 eliminate methanogenic activity for efficient chain elongation reactions⁴. Long-chain
496 alcohol producers are also potentially competitors, and their enrichment leads to over-
497 conversion of substrates to by-products such as butanol and hexanol, resulting in a
498 shortage of electron donors⁷. In this study, the cumulative methane production and
499 maximum content of long-chain alcohols are substantially reduced by AlkBC-ferrate,
500 in comparison with the control, AlkBC or ferrate (Fig. 1b and Fig. 1d). Microbial
501 community analysis further confirms the enrichment of hydrolytic, acidogenic, and
502 chain-elongating bacteria (e.g., *Macellibacteroides sp.*, *Trichococcus sp.*) alongside the
503 suppression of methanogens (i.e., *Methanobacterium sp.*) (Fig. 5). Hence, AlkBC-
504 ferrate effectively modulates microbial competition, selectively inhibiting undesirable
505 microbes while preserving functional populations.

506 Ferrate oxidation increases the number of oxygen-containing functional groups on
507 AlkBC, improving its redox properties and adsorption capacity for metal ions (Fig. 4a-
508 4c). This alteration strengthens interactions between AlkBC and ferrate-derived
509 particles (mainly Fe₂O₃) (Fig. 4d). Previous studies reported that Fe₂O₃ dosing elevated

510 MCFA production from 3793 to 9162 mg COD L⁻¹¹⁶, while Fe₂O₃ loading enhanced the
511 electron transfer capacity of digestate BC⁵¹. Hence, AlkBC is synergistically modified
512 by ferrate oxidation and in-situ Fe₂O₃ deposition in this work. Electron transfer system
513 activity and cyclic voltammetry curves confirm that AlkBC-ferrate triggers more rapid
514 extracellular electron transport (Fig. 4e and Supplementary Fig. 4c). Additionally,
515 AlkBC provides microbial attachment sites, while iron oxides on AlkBC interact with
516 electronegative EPS, promoting microbial aggregation in chain elongation system (Fig.
517 4g). The enhanced microbial aggregation can facilitate the establishment of electrical
518 connections and electron transfer between microorganisms⁶⁰. Consequently, ferrate-
519 modified AlkBC improves the chain elongation bioprocess with Fe₂O₃ as the active iron
520 component on its surface, resulting in significantly higher MCFA production than
521 control, raw AlkBC and ferrate-reduced particles (Fig. 4f).

522 **Implications**

523 This study presents an innovative and sustainable technology for in-situ upgrading
524 of WAS-derived SCFAs into higher-value MCFAs. The AlkBC-ferrate system reaches
525 10495.0 mg COD L⁻¹ MCFAs, surpassing prior records achieved by free ammonia (i.e.,
526 8300 mg COD L⁻¹)²⁹, ferrate (i.e., 8106.3 mg COD L⁻¹)¹³, electro-fermentation (i.e.,
527 1320 mg COD L⁻¹)⁶¹ and Fe₃O₄ (i.e., 7953.6 mg COD L⁻¹)³⁵. A preliminary economic
528 assessment was performed based on sludge reduction and yield of liquid products
529 (Supplementary Table 2). The revenues of fermentation products in the control, AlkBC,
530 ferrate and AlkBC-ferrate groups can offset the costs of chemical dosing, AlkBC
531 preparation and sludge disposal, with the net economic benefit reaching \$29, \$58, \$210

532 and \$680 per tonne of dry sludge, respectively. Notably, the cost input of AlkBC-ferrate
533 technology is mainly derived from potassium ferrate, which is much higher than AlkBC
534 preparation. The combination not only reduces the ferrate dosage, but also achieves
535 higher MCFA production and sludge reduction. However, the potential challenges for
536 scaling up the AlkBC-ferrate technology remain the cost of ferrate and source of
537 electron donor. Future research should prioritize developing cost-effective methods for
538 in-situ ferrate generation and confirming the efficiency of endogenous ethanol
539 production from pretreated WAS, to reduce reliance on commercial chemicals (e.g.,
540 potassium ferrate and ethanol) and avoid complex processes of utilizing other biowaste-
541 derived electron donors. Besides, integrating this pretreatment into a broader
542 biorefinery framework (e.g., co-producing MCFAs and biogas) will further enhance
543 overall economic viability by maximizing resource valorization^{62,63}. Following MCFA
544 extraction, the fermentation residue undergoes anaerobic digestion for methane-rich
545 biogas production, where the retained ferrate-modified AlkBC continuously promotes
546 electron transfer to boost methanogenesis⁶⁴. Ultimately, iron (hydr)oxides derived from
547 ferrate reduction accumulate in the digestate, allowing magnetic recovery of vivianite
548 ($\text{Fe}_3(\text{PO}_4)_2 \cdot 8\text{H}_2\text{O}$)⁶⁵. It is a high-value phosphate product, thus closing the iron loop.
549 This synergistic integration maximizes resource recovery (namely, MCFAs, biogas,
550 phosphorus) from WAS, while incorporating biochar functionality and iron components
551 within a circular economy framework.

552

553 Data Availability Statement

554 The data supporting the findings of this study are available in the main text and
555 the Supplementary Information. The raw sequencing data generated in this study are
556 available in the NCBI Sequence Read Archive database under accession number
557 PRJNA1346931.

ARTICLE IN PRESS

558 **References**

- 559 1. K, A. & Selvasembian, R. Insights into the recent advances of chemical pretreatment
560 of waste activated sludge to enhance biomethane production. *Journal of*
561 *Environmental Chemical Engineering* **12**, 113999 (2024).
- 562 2. Zhao, H. *et al.* Solar-driven sewage sludge electroreforming coupled with biological
563 funnelling to cogenerate green food and hydrogen. *Nature Water* **2**, 1102-1115
564 (2024).
- 565 3. Battista, F. *et al.* Treatment of food processing wastes for the production of medium
566 chain fatty acids via chain elongation. *Environmental Technology & Innovation* **33**,
567 103453 (2024).
- 568 4. Wang, Y., Wei, W., Wu, S.-L. & Ni, B.-J. Zerovalent Iron Effectively Enhances
569 Medium-Chain Fatty Acids Production from Waste Activated Sludge through
570 Improving Sludge Biodegradability and Electron Transfer Efficiency.
571 *Environmental Science & Technology* **54**, 10904-10915 (2020).
- 572 5. Chaitanya, N. K. & Chatterjee, P. Medium chain fatty acid production from CO₂ in
573 integrated dark fermentation-microbial electrosynthesis reactor. *Bioresource*
574 *Technology* **426**, 132371 (2025).
- 575 6. San-Valero, P., Abubakar, H. N., Veiga, M. C. & Kennes, C. Effect of pH, yeast
576 extract and inorganic carbon on chain elongation for hexanoic acid production.
577 *Bioresource Technology* **300**, 122659 (2020).
- 578 7. Wang, Y. *et al.* Medium-chain fatty acids production from sewage sludge through
579 anaerobic fermentation: A critical review. *Chemical Engineering Journal* **477**,
580 147138 (2023).
- 581 8. Gunawan, G., Basid Adiwibawa Prasetya, N. & Adi Wijaya, R. Electrosynthesis of
582 ferrate from iron waste and seawater salts as Antibacterials for water pollutant
583 treatment. *Chemical Engineering Journal* **498**, 155422 (2024).
- 584 9. Cao, J.-Y. *et al.* Ferrate(VI)-based synergistic oxidation processes (Fe(VI)-SOPs):
585 Promoted reactive species production, micropollutant/microorganism elimination,
586 and toxicity reduction. *Chemical Engineering Journal* **489**, 151180 (2024).
- 587 10. Jiang, J.-Q., Panagouloupoulos, A., Bauer, M. & Pearce, P. The application of
588 potassium ferrate for sewage treatment. *Journal of Environmental Management* **79**,
589 215-220 (2006).
- 590 11. Luo, M. *et al.* Insights into the role of in-situ and ex-situ hydrogen peroxide for
591 enhanced ferrate(VI) towards oxidation of organic contaminants. *Water Research*
592 **203**, 117548 (2021).
- 593 12. Mao, Y. *et al.* Removal of micro organic pollutants in high salinity wastewater by
594 comproportionation system of Fe(VI)/Fe(III): Enhancement of chloride and
595 bicarbonate. *Water Research* **214**, 118182 (2022).
- 596 13. Wang, Y. *et al.* Ferrate pretreatment-anaerobic fermentation enhances medium-
597 chain fatty acids production from waste activated sludge: Performance and
598 mechanisms. *Water Research* **229**, 119457 (2023).
- 599 14. Robert *et al.* Ferrate(VI)-Induced Arsenite and Arsenate Removal by In Situ
600 Structural Incorporation into Magnetic Iron(III) Oxide Nanoparticles.

- 601 *Environmental Science & Technology Es & T* (2013).
- 602 15. Goodwill, J. E., Jiang, Y., Reckhow, D. A., Gikonyo, J. & Tobiason, J. E.
603 Characterization of Particles from Ferrate Preoxidation. *Environmental Science &*
604 *Technology* **49**, 4955-4962 (2015).
- 605 16. Wang, Y. *et al.* Ferric oxide stimulates medium-chain carboxylic acids synthesis
606 from waste activated sludge via ethanol-driven chain elongation: Mechanisms and
607 implications. *Journal of Cleaner Production* **389**, 136044 (2023).
- 608 17. Dong, F. *et al.* Simultaneous generation of free radicals, Fe(IV) and Fe(V) by ferrate
609 activation: A review. *Chemical Engineering Journal* **481**, 148669 (2024).
- 610 18. Li, L. *et al.* Efficient Volatile Fatty Acids Production from Waste Activated Sludge
611 after Ferrate Pretreatment with Alkaline Environment and the Responding
612 Microbial Community Shift. *ACS Sustainable Chemistry & Engineering* **6**, 16819-
613 16827 (2018).
- 614 19. Fakhar, A., Canatoy, R. C., Galgo, S. J. C., Rafique, M. & Sarfraz, R. Advancements
615 in modified biochar production techniques and soil application: a critical review.
616 *Fuel* **400**, 135745 (2025).
- 617 20. Gao, Y. *et al.* Intrinsic properties of biochar for electron transfer. *Chemical*
618 *Engineering Journal* **475**, 146356 (2023).
- 619 21. Tian, S.-Q., Wang, L., Liu, Y.-L. & Ma, J. Degradation of organic pollutants by
620 ferrate/biochar: Enhanced formation of strong intermediate oxidative iron species.
621 *Water Research* **183**, 116054 (2020).
- 622 22. Wu, S.-L. *et al.* Revealing the Mechanism of Biochar Enhancing the Production of
623 Medium Chain Fatty Acids from Waste Activated Sludge Alkaline Fermentation
624 Liquor. *Acs Es&T Water* **1**, 1014-1024 (2021).
- 625 23. Lou, T., Yin, Y. & Wang, J. Influence of adding strategy of biochar on medium-
626 chain fatty acids production from sewage sludge. *Chemosphere* **354**, 141660
627 (2024).
- 628 24. Chen, L. *et al.* Functionalized biochars with highly-efficient malachite green
629 adsorption property produced from banana peels via microwave-assisted pyrolysis.
630 *Bioresource Technology* **376**, 128840 (2023).
- 631 25. Gao, X. *et al.* Performance and mechanism of biochar pretreatment on improving
632 short-chain fatty acids production from anaerobic fermentation of waste activated
633 sludge. *Journal of Environmental Chemical Engineering* **12**, 114828 (2024).
- 634 26. Li, X. Y. & Yang, S. F. Influence of loosely bound extracellular polymeric
635 substances (EPS) on the flocculation, sedimentation and dewaterability of
636 activated sludge. *Water Research* **41**, 1022-1030 (2007).
- 637 27. Hu, T. *et al.* Micro-mechanism of rhamnolipid promoting acid production during
638 anaerobic digestion: protein structures, metagenomics and molecular dynamics
639 simulations. *Water Research* **283**, 123795 (2025).
- 640 28. Maleki, E., Yu, D. & Parker, W. Assessment of active heterotrophs and hydrolytic
641 enzyme activities as indicators of hydrolysis rates in anaerobic digestion of mixed
642 primary and waste activated sludges. *Journal of Environmental Chemical*
643 *Engineering* **13**, 115302 (2025).
- 644 29. Wang, Y. *et al.* Improving Medium-Chain Fatty Acid Production from Anaerobic

- 645 Fermentation of Waste Activated Sludge Using Free Ammonia. *Acs Es&T*
646 *Engineering* **1**, 478-489 (2021).
- 647 30. Miner, G. Standard Methods for the Examination of Water and Wastewater, 21st
648 Edition. *Journal American Water Works Association*, 130 (2006).
- 649 31. Tantray, J. A., Mansoor, S., Wani, R. F. C. & Nissa, N. U. in *Basic Life Science*
650 *Methods* (eds Javeed Ahmad Tantray, Sheikh Mansoor, Rasy Fayaz Choh Wani,
651 & Nighat Un Nissa) 65-67 (Academic Press, 2023).
- 652 32. Prakash Jain, B., Pandey, S. & Goswami, S. K. in *Protocols in Biochemistry and*
653 *Clinical Biochemistry (Second Edition)* (eds Buddhi Prakash Jain, Shweta Pandey,
654 & Shyamal K. Goswami) 35-36 (Academic Press, 2025).
- 655 33. Chubar, N., Gerda, V., Szlachta, M. & Yablokova, G. Effect of Fe oxidation state
656 (+2 versus +3) in precursor on the structure of Fe oxides/carbonates-based
657 composites examined by XPS, FTIR and EXAFS. *Solid State Sciences* **121**,
658 106752 (2021).
- 659 34. Mishra, S. & Kumar Tiwari, M. Adsorptive removal of diclofenac on nanoporous
660 anoxic sewage sludge biochar: Investigating the influence of carbonization
661 temperature, residence time and specific Fe(III) infusion. *Separation and*
662 *Purification Technology* **354**, 129322 (2025).
- 663 35. Wang, Y. *et al.* New insight into mechanisms of ferroferric oxide enhancing
664 medium-chain fatty acids production from waste activated sludge through
665 anaerobic fermentation. *Bioresource Technology* **360**, 127629 (2022).
- 666 36. Sharma, V. K. Ferrate(VI) and ferrate(V) oxidation of organic compounds: Kinetics
667 and mechanism. *Coordination Chemistry Reviews* **257**, 495-510 (2013).
- 668 37. Rush, J. D. & Bielski, B. H. J. Pulse radiolysis studies of alkaline iron(III) and
669 iron(VI) solutions. Observation of transient iron complexes with intermediate
670 oxidation states. *Journal of the American Chemical Society* **108**, 523-525 (1986).
- 671 38. Antonicelli, G. *et al.* Harnessing an adapted strain of *Clostridium carboxidivorans*
672 to unlock hexanol production from carbon dioxide and hydrogen in elevated-
673 pressure stirred tank reactors. *Bioresource Technology* **418**, 131966 (2025).
- 674 39. Lai, J. *et al.* Promotion of aromatic amino acids of extracellular polymeric substance
675 targeted transformation via sulfite mediated iron redox cycling in sludge solid-
676 liquid separation. *Water Research* **266**, 122369 (2024).
- 677 40. Wu, S.-L. *et al.* Unveiling the mechanisms of medium-chain fatty acid production
678 from waste activated sludge alkaline fermentation liquor through physiological,
679 thermodynamic and metagenomic investigations. *Water Research* **169**, 115218
680 (2020).
- 681 41. Cao, W. *et al.* Choline chloride pretreatment on volatile fatty acids promotion from
682 sludge anaerobic fermentation: In-situ deep eutectic solvents-like formation for
683 EPS disintegration and associated microbial functional profiles upregulation.
684 *Chemical Engineering Journal* **467**, 143556 (2023).
- 685 42. Wang, Q. *et al.* Study on short-chain fatty acids production from anaerobic
686 fermentation of waste activated sludge pretreated by alkali-activated ammonium
687 persulfate. *Bioresource Technology* **428**, 132461 (2025).
- 688 43. Chen, Y., Ping, Q., Li, D., Dai, X. & Li, Y. Comprehensive insights into the impact

- 689 of pretreatment on anaerobic digestion of waste active sludge from perspectives of
690 organic matter composition, thermodynamics, and multi-omics. *Water Research*
691 **226**, 119240 (2022).
- 692 44. Li, Y. *et al.* Fe(II) catalyzing sodium percarbonate facilitates the dewaterability of
693 waste activated sludge: Performance, mechanism, and implication. *Water Research*
694 **174**, 115626 (2020).
- 695 45. Sharma, V. K., Zboril, R. & Varma, R. S. Ferrates: Greener Oxidants with
696 Multimodal Action in Water Treatment Technologies. *Accounts of Chemical*
697 *Research* **48**, 182-191 (2015).
- 698 46. Sharma, V. K. *et al.* Reactive High-Valent Iron Intermediates in Enhancing
699 Treatment of Water by Ferrate. *Environmental Science & Technology* **56**, 30-47
700 (2022).
- 701 47. Loures, C. *et al.* Advanced Oxidative Degradation Processes: Fundamentals and
702 Applications. *2035-1755* **5** (2013).
- 703 48. Tian, S.-Q. *et al.* Enhanced Permanganate Oxidation of Sulfamethoxazole and
704 Removal of Dissolved Organics with Biochar: Formation of Highly Oxidative
705 Manganese Intermediate Species and in Situ Activation of Biochar. *Environmental*
706 *Science & Technology* **53**, 5282-5291 (2019).
- 707 49. Jiang, Q. *et al.* Deciphering the effects of engineered biochar on methane production
708 and the mechanisms during anaerobic digestion: Surface functional groups and
709 electron exchange capacity. *Energy Conversion and Management* **258**, 115417
710 (2022).
- 711 50. Lv, X. *et al.* Nickel phosphide nanoarrays decorated on amorphous NiPO_x/Fe(OH)₃:
712 A stable core-shell electrocatalyst for efficient oxygen evolution at large current
713 density. *Chemical Engineering Journal* **475**, 146128 (2023).
- 714 51. Wang, Y. *et al.* Preparation of iron oxide-modified digestate biochar and effect on
715 anaerobic digestion of kitchen waste. *Bioresource Technology* **398**, 130515 (2024).
- 716 52. Yang, Y., Ma, P., Li, Y., Chen, Y. & Zhang, H. Sludge-derived biochar improves
717 sludge electro-dewatering performance: Conductivity analysis. *Colloids and*
718 *Surfaces A: Physicochemical and Engineering Aspects* **701**, 134838 (2024).
- 719 53. Linda *et al.* *Macelibacteroides fermentans* gen. nov., sp. nov., a member of the
720 family Porphyromonadaceae isolated from an upflow anaerobic filter treating
721 abattoir wastewaters. *International journal of systematic and evolutionary*
722 *microbiology* **62**, 2522-2527 (2012).
- 723 54. Pikuta, E. V. *et al.* *Trichococcus patagoniensis* sp nov., a facultative anaerobe that
724 grows at -5 degrees C, isolated from penguin guano in Chilean Patagonia.
725 *International Journal of Systematic and Evolutionary Microbiology* **56**, 2055-2062
726 (2006).
- 727 55. He, Z.-W. *et al.* Freezing-low temperature treatment facilitates short-chain fatty
728 acids production from waste activated sludge with short-term fermentation.
729 *Bioresource Technology* **347** (2022).
- 730 56. He, J. *et al.* Phenol promoted caproate production via two-stage batch anaerobic
731 fermentation of organic substance with ethanol as electron donor for chain
732 elongation. *Water Research* **204**, 117601 (2021).

- 733 57. Zheng, S., Li, M., Liu, Y. & Liu, F. Desulfovibrio feeding Methanobacterium with
734 electrons in conductive methanogenic aggregates from coastal zones. *Water*
735 *Research* **202**, 117490 (2021).
- 736 58. Zhang, H. *et al.* Enhanced ferrate(VI) oxidation of sulfamethoxazole in water by
737 CaO₂: The role of Fe(IV) and Fe(V). *Journal of Hazardous Materials* **425**, 128045
738 (2022).
- 739 59. Wu, Q. *et al.* Medium chain carboxylic acids production from waste biomass:
740 Current advances and perspectives. *Biotechnology Advances* **37**, 599-615 (2019).
- 741 60. Barua, S. & Dhar, B. R. Advances towards understanding and engineering direct
742 interspecies electron transfer in anaerobic digestion. *Bioresource Technology* **244**,
743 698-707 (2017).
- 744 61. Su, W. *et al.* Boosting the biosynthesis of medium-chain fatty acids from waste
745 activated sludge electro-fermentation: Roles of syngas and ethanol serving as co-
746 electron donors. *Journal of Cleaner Production* **502**, 145383 (2025).
- 747 62. Battista, F. & Bolzonella, D. Beyond Anaerobic Digestion: New Perspectives for
748 the Development of a Biorefinery Platform for the Simultaneous Production of
749 Medium-Chain Fatty Acids by Chain Elongation and Biogas from Food Wastes.
750 *ACS Sustainable Chemistry & Engineering* **12**, 15294-15306 (2024).
- 751 63. Battista, F. *et al.* Designing a flexible anaerobic biorefinery for the valorization of
752 red grape marcs into biofuels and biochemicals. *Environmental Technology &*
753 *Innovation* **39**, 104340 (2025).
- 754 64. Jin, H.-Y. *et al.* Deciphering the synergistic effects and mechanisms of biochar and
755 magnetite contained in magnetic biochar for enhancing methane production in
756 anaerobic digestion of waste activated sludge. *Water Research* **282**, 123734 (2025).
- 757 65. Cheng, Y. *et al.* Pyrochar relieved the negative effects of hydrothermal pretreatment
758 of sludge on vivianite production in anaerobic digestion. *Chemical Engineering*
759 *Journal* **516**, 164096 (2025).

760

761 **Acknowledgements**

762 This study was supported by the National Natural Science Foundation of China
763 through project 52400180, and by the China Postdoctoral Science Foundation under
764 Grant Number GZB20240523. Authors are grateful to the research collaboration.

ARTICLE IN PRESS

Author contributions

Yufen Wang: Conceptualization, Investigation, Funding acquisition, Writing - original draft, Writing - review & editing.

Ya Ji: Investigation.

Xiaofeng Luo: Writing - review & editing.

Tingting Zhu: Writing - review & editing.

Bing-Jie Ni: Conceptualization, Writing - review & editing.

Yiwen Liu: Conceptualization, Resources, Writing - review & editing.

Author Information (authors and affiliations, corresponding authors)

Yufen Wang ^a, Ya Ji ^a, Xiaofeng Luo ^a, Tingting Zhu ^a, Bing-Jie Ni ^b, Yiwen Liu ^{a,*}

^a School of Environmental Science and Engineering, Tianjin University, Tianjin 300072, China

^b School of Civil and Environmental Engineering, University of New South Wales, Sydney, New South Wales, 2052, Australia

*Corresponding author

E-mail: yiwen.liu@tju.edu.cn (Y. Liu)

Ethics declarations

Competing interests

The authors declare no competing interests.

ARTICLE IN PRESS

1 **Figure captions**

2 **Fig. 1. Product profiles in the control, alkaline biochar (AlkBC), ferrate and**
3 **AlkBC-ferrate systems during medium-chain fatty acid (MCFA) biosynthesis from**
4 **anaerobic fermentation of waste activated sludge. a** MCFA production, expressed as
5 chemical oxygen demand (COD). **b** Cumulative CH₄ production. **c** Product
6 distributions at the end of anaerobic fermentation. **d** Long-chain alcohol production,
7 expressed as COD. Error bars denote the standard deviations of triplicate experiments.

8

9 **Fig. 2. Dynamics of soluble organics and bound extracellular polymeric substances**
10 **(EPS), protein secondary structure, and enzymatic/metabolic activities during 48-**
11 **hour WAS pretreatment. a** Concentration of proteins and polysaccharides in extracted
12 bound EPS. **b-d** Variations in concentration of proteins, carbohydrates and chemical
13 oxygen demand (COD) in the soluble fraction during pretreatment, with **d** showing the
14 COD distributions in the soluble fraction and extracted bound EPS. **e** Fitting curve of
15 the amide I region (1600–1700 cm⁻¹) in Fourier-transform infrared spectra of soluble
16 organics. **f** Activity of protease and α -glucosidase, ammonia nitrogen release and short-
17 chain fatty acid (SCFA) production. Error bars denote the standard deviations of
18 triplicate experiments.

19

20 **Fig. 3. Mechanisms of sludge dissolution and organic biotransformation in the**
21 **alkaline biochar (AlkBC)-ferrate pretreatment system. a** Soluble protein
22 concentration during 48-hour pretreatment. **b** Concentration of soluble chemical

23 oxygen demand (COD) after 12-hour pretreatment. **c** Decay profiles of Fe(VI) in
24 distilled water following addition of ferrate alone or AlkBC-ferrate, with inset showing
25 enlarged ultraviolet-visible spectra for the AlkBC-ferrate group. **d** Degradation
26 efficiency of bovine serum albumin, and short-chain fatty acid (SCFA) concentrations
27 from acidification of amino acids and glucose in synthetic wastewater experiments.
28 Error bars denote the standard deviations of triplicate experiments.

29

30 **Fig. 4. Structural properties of ferrate-modified alkaline biochar (AlkBC) and its**
31 **enhancement of chain elongation.** **a** Fourier-transform infrared spectra of raw AlkBC
32 and ferrate-modified AlkBC. **b, c** C1s spectra from X-ray photoelectron spectroscopy
33 for raw AlkBC and ferrate-modified AlkBC. **d** Fe2p spectra from X-ray photoelectron
34 spectroscopy for Fe element on the surface of ferrate-modified AlkBC. **e** Electron
35 transport system activity of different groups during WAS fermentation. **f** Medium-chain
36 fatty acid (MCFA) production, expressed as chemical oxygen demand (COD), in chain
37 elongation biostep with the presence of different Fe and/or AlkBC, assessed by
38 synthetic wastewater experiments. **g** Scanning electron microscopy images of sludge
39 samples from the chain elongation experiment, including the control, raw AlkBC,
40 ferrate-reduced particles, and ferrate-modified AlkBC groups. Error bars denote the
41 standard deviations of triplicate experiments.

42

43 **Fig. 5. Microbial community structure and associated functional taxa profiles of**
44 **the control, alkaline biochar (AlkBC), ferrate and AlkBC-ferrate groups after**

45 **anaerobic fermentation. a** Phylum-level taxonomic composition of microbial
46 communities, where circle colors denote the different pretreatment conditions (i.e.,
47 Control, AlkBC, ferrate, and AlkBC-ferrate). **b** Heatmap of genus-level functional taxa
48 involved in key bioprocesses.

49

50 **Fig. 6. Schematic diagram of mechanisms.** Stage-optimized modulation of sludge-to-
51 MCFA conversion driven by the AlkBC-ferrate strategy.

52

53

54

55

56 **Editor's Summary:**

57 Yufen Wang and colleagues report a synergistic alkaline biochar-ferrate technique to enhance
58 medium-chain fatty acid (MCFA) production from sludge by stage-optimized modulation. This
59 strategy overcomes dual bottlenecks in sludge-to-MCFA conversion.

60

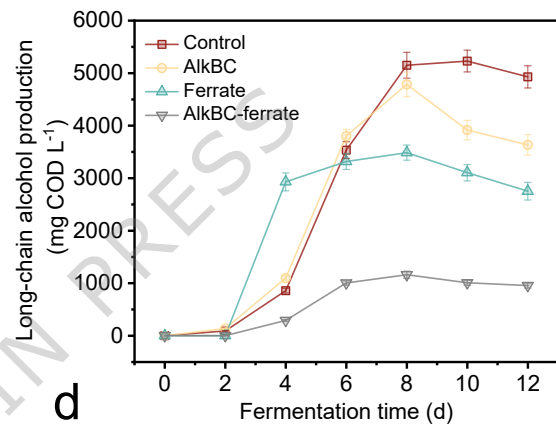
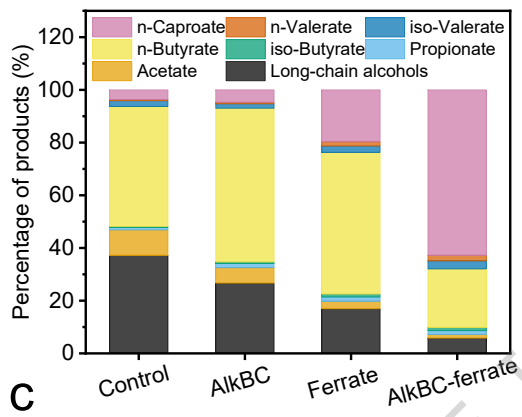
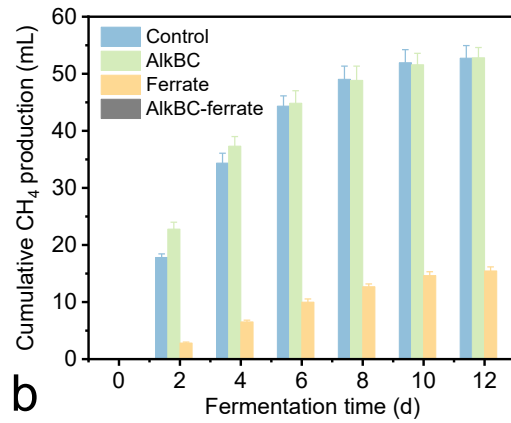
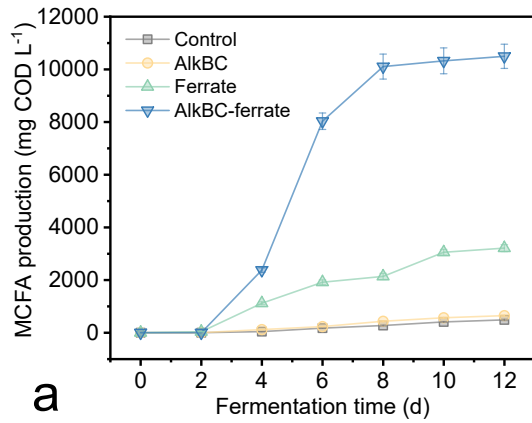
61

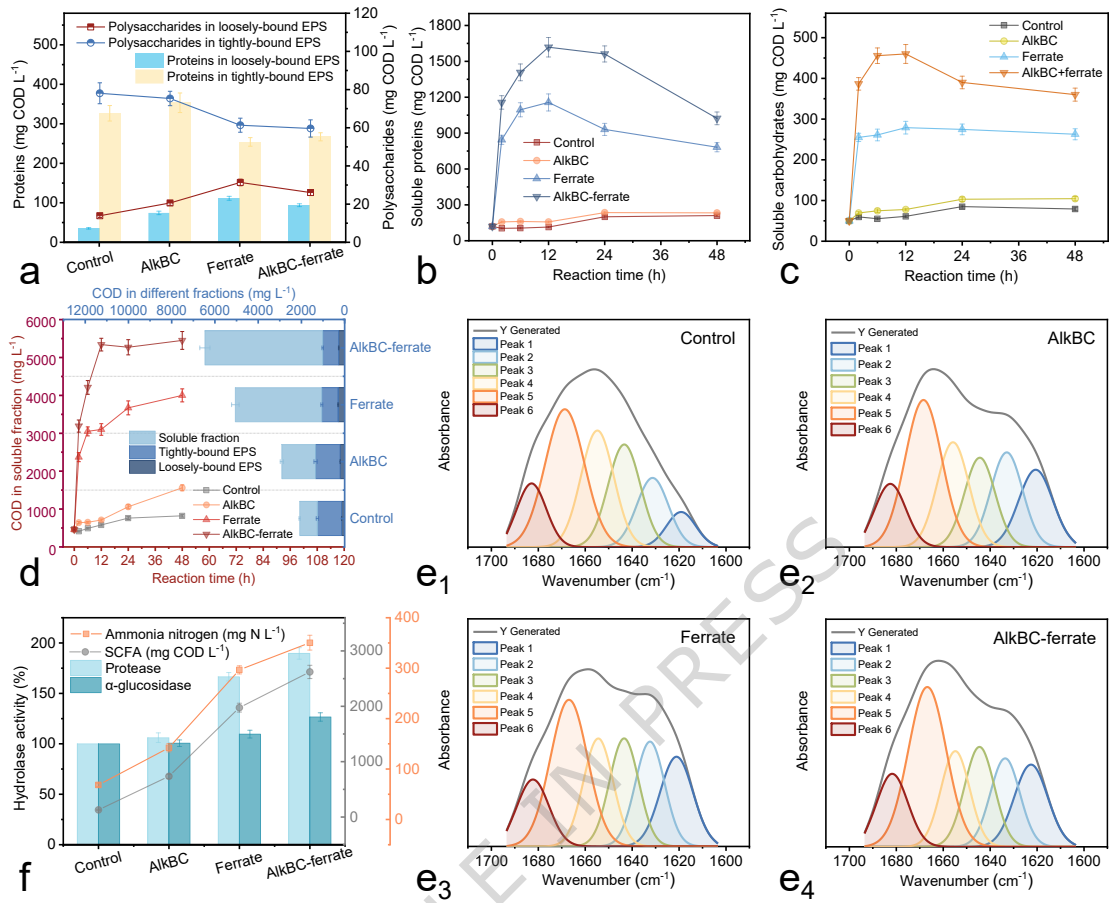
62 **Peer review information:**

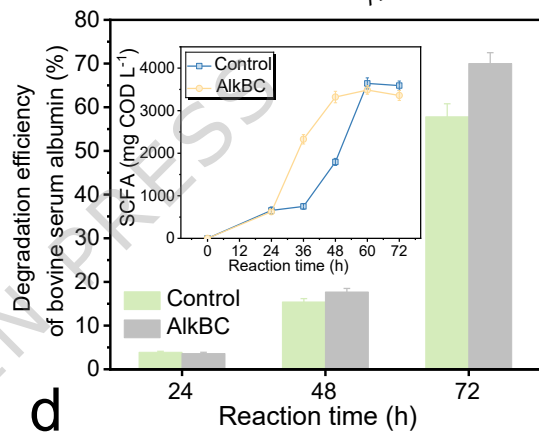
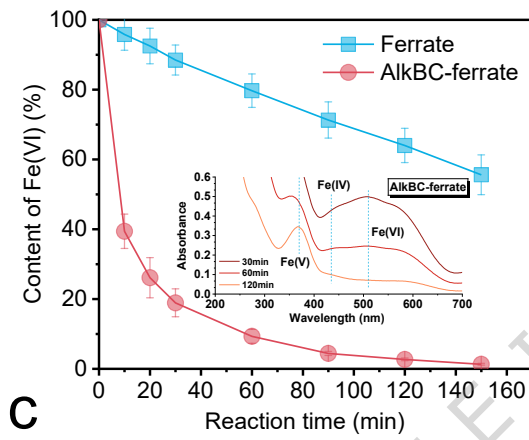
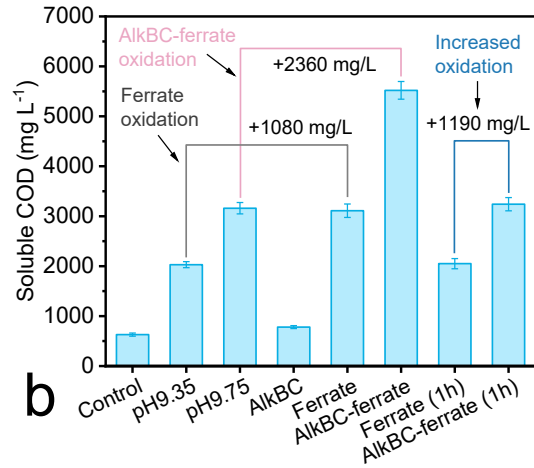
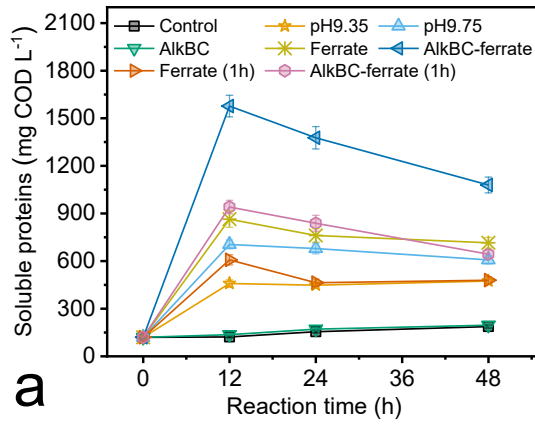
63 *Communications Engineering* thanks Federico Battista and the other, anonymous, reviewer(s)
64 for their contribution to the peer review of this work. Primary Handling Editors: [Philip
65 Coatsworth]

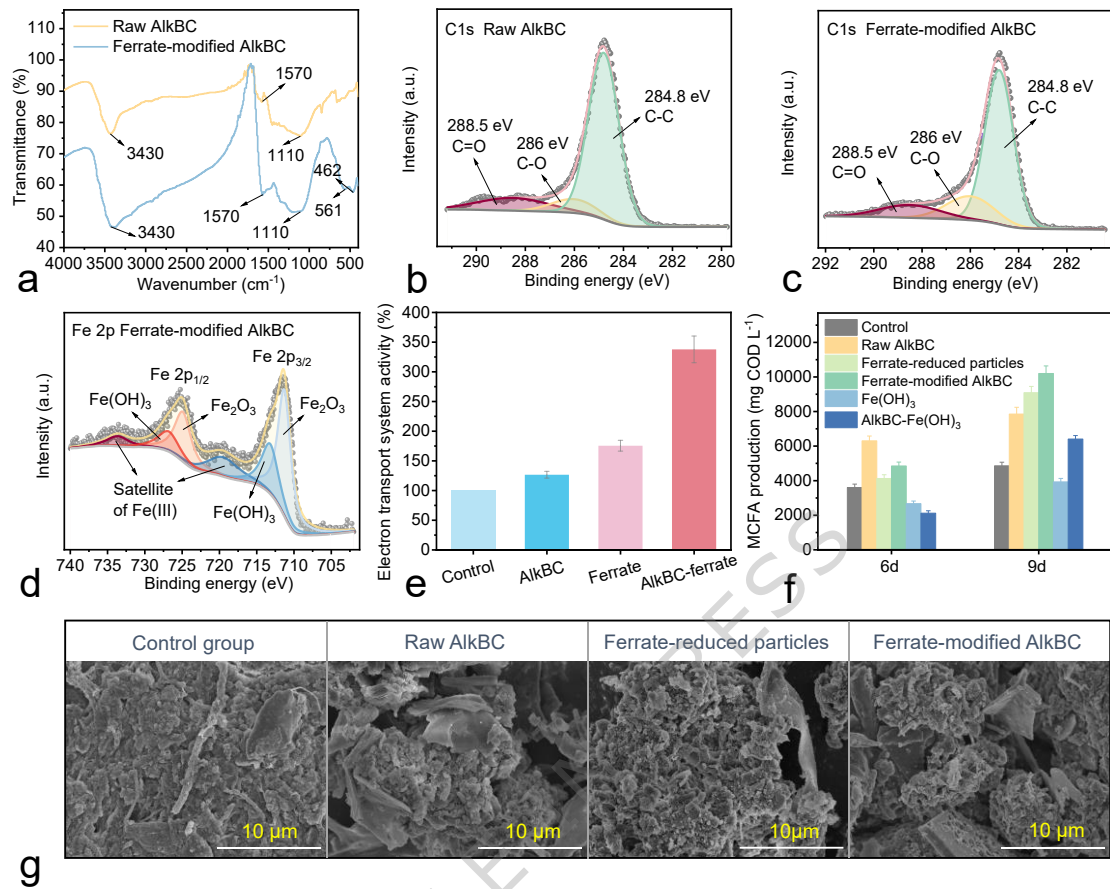
66

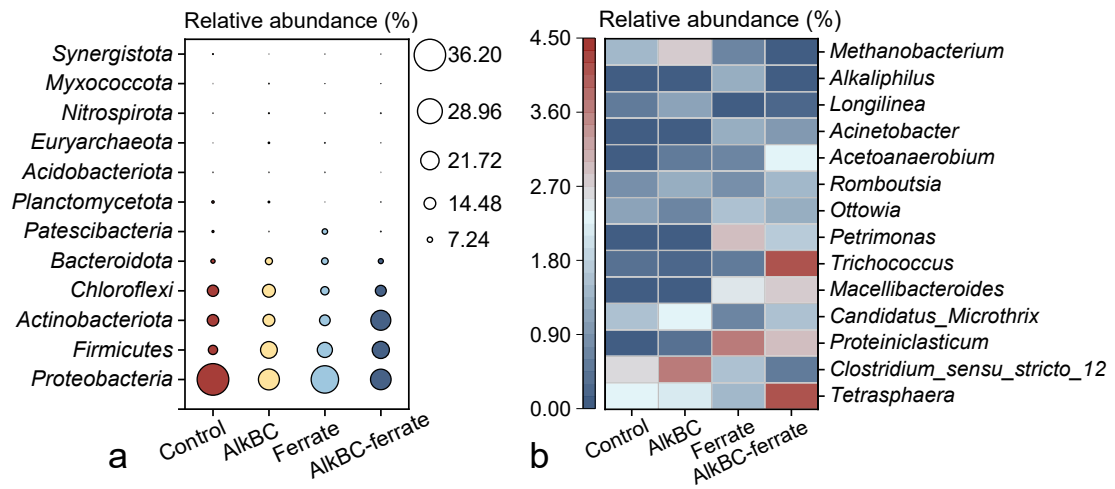
67











ARTICLE IN PRESS

